Eur Biophys J (2009) 38:185–198
DOI 10.1007/s00249-008-0369-x

ORIGINAL PAPER

Ligand unbinding pathways from the vitamin D receptor studied by molecular dynamics simulations

Mikael Peräkylä

Received: 18 April 2008 / Revised: 25 August 2008 / Accepted: 28 August 2008 / Published online: 3 October 2008

Abstract Molecular dynamics simulation techniques have been used to study the unbinding pathways of 1α,25-dihydroxyvitamin D_3 from the ligand-binding pocket of the vitamin D receptor (VDR). The pathways observed in a large number of relatively short (<200 ps) random acceleration molecular dynamics (RAMD) trajectories were found to be in fair agreement, both in terms of pathway locations and deduced relative preferences, compared to targeted molecular dynamics (TMD) and streered molecular dynamics simulations (SMD). However, the high-velocity ligand expulsions of RAMD tend to favor straight expulsion trajectories and the observed relative frequencies of different pathways were biased towards the probability of entering a particular exit channel. Simulations indicated that for VDR the unbinding pathway between the H1–H2 loop and the β-sheet between H5 and H6 is more favorable than the pathway located between the H1–H2 loop and H3. The latter pathway has been suggested to be the most likely unbinding path for thyroid hormone receptors (TRs) and a likely path for retinoic acid receptor. Ligand entry/exit through these two pathways would not require displacement of H12 from its agonistic position. Differences in the packing of the H1, H2, H3 and β-sheet region explain the changed relative preference of the two unbinding pathways in VDR and TRs. Based on the crystal structures of the ligand binding domains of class 2 nuclear receptors, whose members are VDR and TRs, this receptor class can be divided in two groups according to the packing of the H1, H2, H3 and β-sheet region.

Keywords Molecular dynamics · Nuclear receptor · Random acceleration molecular dynamics · Steered dynamics · Targeted molecular dynamics · Vitamin D receptor

Introduction

The nuclear receptor (NR) superfamily of ligand-modulated transcription factors has 48 human members, which regulate genes involved in diverse processes, such as reproduction, development and inflammation and, therefore, have attracted broad scientific and pharmaceutical interest (Chawla et al. 2001). NRs were first recognized as the receptors for the steroid hormones estradiol (ERα and β), progesterone (PR), testosterone (AR), cortisol (GR) and aldosterol (MR), for thyroid hormone (TRα and β) and for the biologically active forms of the fat-soluble vitamins A and D, all-*trans* retinoic acid (RARα, β and γ) and 1α,25-dihydroxyvitamin D_3 receptor (VDR). NRs have a modular structure of three main domains: the N-terminal AF-1 domain, the central DNA-binding domain and the C-terminal ligand-binding (LBD) domain. The overall architecture of the LBD is well conserved between the various family members, nonetheless diverges sufficiently to guarantee selective ligand recognition as well as accommodate the broad spectrum of NR ligand structures (Bain et al. 2007). The LBD consists of 250–300 amino acids in 11–13 α-helices (Fig. 1a) (Rochel et al. 2000). Ligand binding causes a conformational change within the LBD, whereby, at least in the case of endocrine NRs, helix 12 (H12), the most C-terminal α-helix, closes the ligand-binding pocket (LBP)

Electronic supplementary material The online version of this article (doi:10.1007/s00249-008-0369-x) contains supplementary material, which is available to authorized users.

M. Peräkylä (✉)
Department of Biosciences, University of Kuopio,
P.O. Box 1627, 70211 Kuopio, Finland
e-mail: mikael.perakyla@uku.fi

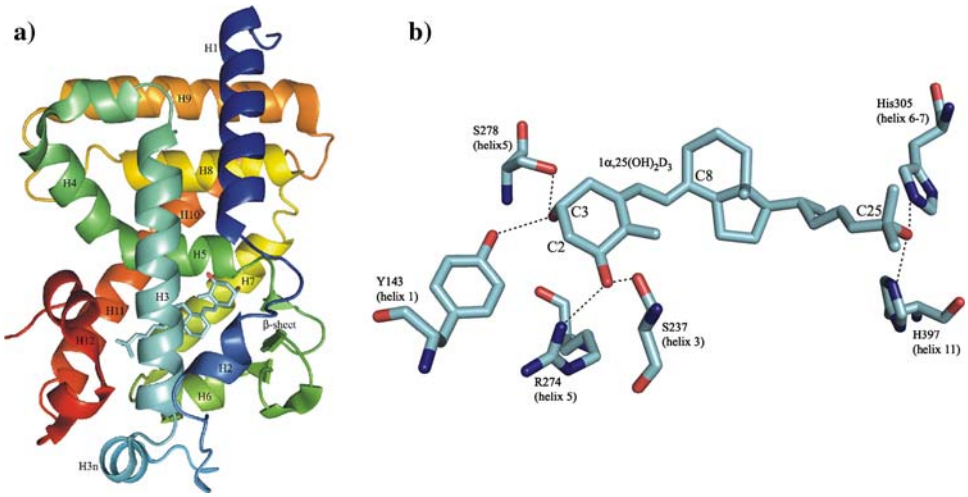

Fig. 1 Structure of VDR LBD and VDR–VD3 interactions

via a "mouse-trap like" intramolecular folding event (Li et al. 2003; Moras and Gronemeyer 1998). There exists increasing amount of evidence that the simple model of H12 acting as a two-state molecular switch needs to be, at least somewhat, modulated (Shiau et al. 2002). For example, ligands have been found to affect differently the conformational dynamics of ERα (Hurth et al. 2004) and modulate ERα and ERβ activities by mechanisms involving subtle differences in receptor–ligand interactions (Margeat et al. 2003; Nettles et al. 2004). Recent studies of peroxisome proliferator-activated receptor (PPAR) γ have nicely demonstrated how partial agonists activate the receptor using a H12 independent mechanism by inducing unique changes to the dynamics of the LBD (Bruning et al. 2007; Einstein et al. 2008).

The NR crystal structures have strongly indicated that ligand entry/exit is regulated by H12 position, although alternative entry/exit pathways have been suggested (Nolte et al. 1998; Wagner et al. 1995). Computational methods based on molecular dynamics (MD) simulations suite very well in identifying qualitatively and even quantitatively ligand exit (entry) channels from protein LBPs (Aird et al. 2007; Gullingsrud et al. 1999; Isralewitz et al. 2001; Jarzynski 1997; Lau and Roux 2007; Park et al. 2003; Xiong et al. 2006). Such information, which is very difficult to obtain experimentally, provides fundamental understanding of protein function but could also add substantial information to rational drug design process where, quite naturally, the protein–ligand interactions have traditionally been the main focus. Ligand exit from NR LBP has been studied using different computational protocols. Kosztin et al. (1999) used the steered molecular dynamics (SMD) (Isralewitz et al. 2001; Izrailev et al. 1998) simulations to study the unbinding of all-*trans* retinoic acid from the LBP of RARγ through three pathways, chosen by visual inspection of the crystal structure. It was suggested, that there exist two plausible entry/exit pathways, one close to H12 and another one between the H1–H2 loop and H3. Blondel et al. (1999) used enhanced sampling molecular dynamics (ESMD), which is a multiple-copy approach, to simulate the escape mechanism of all-*trans* retinoic acid from the LBP of RARγ. Another enhanced sampling method, locally enhanced sampling (LES) MD was applied to study receptor dimerization mediated ligand dissociation from ERα (Sonoda et al. 2008) and to reveal three distinctive ligand dissociation pathways from the TRα and β (Martínez et al. 2005). The exit path having opening between the H1–H2 loop and H3 identified in the latter work was later found, on the basis of force profiles obtained from SMD simulations, to be the most likely ligand unbinding pathway for TRα and β (Martínez et al. 2006). Interestingly, different ligands were found to prefer different exit/entry paths suggesting that this knowledge could be used in designing better TR ligands. Random acceleration molecular dynamics (RAMD) (Ludemann et al. 2000) has also been applied to study the exit pathways from the LBP of RARγ (Carlsson et al. 2006). In this investigation, the exit pathway between the H1–H2 loop and H3 was also found, in addition to three other pathways. The multiple copy dynamics (LES, ESMD) and RAMD, as well as the targeted molecular dynamics (TMD) (Schlitter et al. 1993), which has been applied to ligand unbinding simulations from the LBP of PPARγ (Genest et al. 2008), are suitable for objective exploration of possible ligand entry/exit pathways as in these methods ligands randomly explore the weaknesses of the LBP. In contrast, SMD involves pulling of a ligand out of the LBP using an external force along a route that is chosen in advance. On the other hand, a clear strength of SMD is that it provides force profiles, which can be used to deduce the likelihood of the tested pathways and even to calculate free energy profiles for direct comparison between the alternative pathways and even with experimental on/off rates (Aird et al. 2007; Jarzynski 1997; Park et al. 2003).

The common first problem in entry/exit pathway studies is how to objectively find the most likely pathways, which could then be studied in more detail with quantitative computational simulation approaches like the SMD. The purpose of this work is to study how rather short RAMD ligand expulsion simulations suite for efficient and quick exit channel exploration. To this end, a large number of RAMD trajectories were calculated for the unbinding of the natural VDR ligand, 1α,25-dihydroxyvitamin D_3 (VD3), from the VDR LBP. To compare the exit pathways and pathway frequencies observed in short RAMD simulations, reference simulations were done using the TMD and SMD methods. The reference slow-velocity unbinding pathways were calculated using the TMD method, and the quantitative estimates of how demanding the found unbinding pathways are were deduced from the force profiles of SMD unbinding simulations. In addition, comparison is made between the unbinding pathways found for VDR and those found earlier for other NRs. Finally, crystal structures of several NR LBDs were analyzed to generalize the conclusions made on the basis of VDR simulations of this work and those done earlier for other NRs.

Materials and methods

MD simulations

The initial coordinates of VDR were obtained from the crystal structure of the VDR–LBD–MC1288 complex (Protein Data Bank entry 1IE9) determined to 1.8 Å resolution (Tocchini-Valentini et al. 2001). The four residues missing from the C-terminus (424–427) were built in an α-helical conformation ($\phi = -57°$, $\psi = -47°$). VD3 was placed to the ligand-binding pocket using the VDR–LBD–VD3 crystal structure (Protein Data Bank entry 1DB1) as a model (Rochel et al. 2000).

For the energy minimizations and molecular dynamics (MD) simulations the VDR–VD3 complex was solvated by TIP3P water molecules in a periodic box of ~61 × 69 × 86 Å. Crystallographic water molecules were included in the simulation system. The water molecules, counter ions (six Na^+ ions) and hydrogen atoms of the simulation system were first energy-minimized for 1,000 steps, heated to 300 K in 5 ps, and equilibrated by 45 ps at constant volume and temperature of 300 K. After that the system was minimized for 1,000 steps, the temperature was increased to 300 K in 5 ps, and equilibrated for 60 ps while restraining the six residues (Tyr143, Ser237, Ser278, Arg274, His305 and His397, Fig. 1b) forming hydrogen bonds with VD3 to their initial positions using a harmonic potential of 1 kcal mol^{-1} $Å^{-2}$. After that simulation was continued without restraints for 2.2 ns. Equilibration and production simulations were carried out at constant pressure (1 atm) and temperature (300 K). In the simulations the electrostatics were treated using the particle-mesh Ewald method. A timestep of 1.5 fs was used, and bonds involving hydrogen atoms were constrained to their equilibrium lengths using the SHAKE algorithm (Ryckaert et al. 1977).

RAMD simulations

Ligand unbinding simulations of the VDR–LBD–VD3 system were done using the RAMD (Ludemann et al. 2000) and TMD (Schlitter et al. 1994) methods. In the RAMD method, a randomly oriented force is added to the center of mass of the ligand. The direction of the force is kept constant for a certain number of MD steps (N). If, after N MD steps, the ligand has moved less than the minimum distance (r_{min}), a new direction is chosen randomly, otherwise the same direction is maintained for another N steps. RAMD simulations were stopped when ligand had moved more than 40 Å from the starting position. In all the RAMD simulations, the magnitude of the random force (k) was 24.0 kcal mol^{-1} $Å^{-1}$. Five starting structures (SS1–SS5) saved at 0.6, 1.0, 1.4, 1.8 and 2.2 ns of the 2.2 ns MD simulation were used in the RAMD and TMD simulations. For each starting structure eight simulations starting with different randomly selected directions of the initial force were done using four different RAMD parameter sets having different r_{min} and N values (Table 1). This resulted in 32 RAMD simulations for each of the five starting structures and a total of 160 RAMD simulations. In addition, 40 RAMD simulations were done using the parameter set 4 for each starting structure, resulting in a total of 200 simulations.

TMD simulations

In the TMD simulations, an additional energy term was added to the energy function proportional to the square of the difference between the mass-weighted root mean square deviation (RMSD) of the ligand non-hydrogen atoms in a current VDR–VD3 structure compared to the reference VDR–VD3 structure (starting structure), calculated after RMS fitting the backbone atoms of residues 127–141,

Table 1 RAMD parameter sets 1–4

Set	r_{min}(Å)	N	k (kcal mol^{-1} $Å^{-1}$)
1	0.1	40	24
2	0.1	60	24
3	0.05	80	24
4	0.2	100	24

225–274 and 304–403 of the two complexes, and the target RMSD. The residues used in the fitting exclude the most flexible parts of VDR. In the beginning of TMD simulations, the target RMSD was 0.0 Å, and as the simulations proceeded, the target RMSD was increased linearly at different rates (0.009–0.044 Å ps^{-1}) to 22.0 Å. For each starting structure (SS1–SS5) eight TMD simulations with different force constants of the added energy term (1–4 kcal mol^{-1} $Å^{-2}$) were done. This resulted in total of 40 TMD simulations with ligand expulsion times between 0.5 and 2.5 ns.

SMD simulations

On the basis of RAMD and TMD simulations five most frequently observed ligand unbinding paths, A1, A2, B1, B2 and C (Fig. 2a–c), were chosen for SMD simulations. In the SMD simulations, ligand was pulled towards a point outside the protein surface close to the entrance of the selected pathway. The force constant of the external harmonic force moving with the velocity of 0.018 Å ps^{-1} exerted on the ligand was 5 kcal mol^{-1} $Å^{-2}$. Simulation times were 0.9–1.1 ns depending on the exit path. The force was applied to the ligand carbon atom closest to the outer surface entrance of each pathway (A: C25, B: C3, C: C2, Fig. 1b). For the SMD simulations, which were done in constant volume conditions, 300 ps constant volume equilibration was done starting from the 0.6 ns structure (SS1) of the constant pressure VDR–VD3 MD simulation. Seven simulations, separated by 15 ps of constant volume equilibration, were carried out for each of the five exit paths. To prevent translation and rotation of the protein harmonic constraints with a force constant of 0.5 kcal mol^{-1} $Å^{-2}$ were applied to Cα atoms of Leu219 and Leu222 of H3n and Leu333 and Ile336 of H8. These Cα atoms are located at least 15 Å from bound VD3.

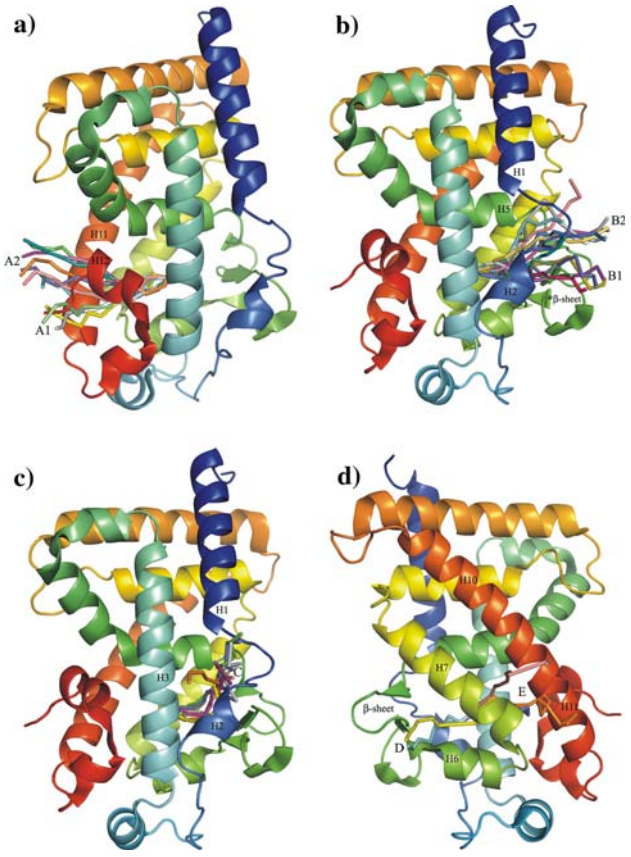

Fig. 2 Ligand unbinding trajectories (**a**) A1 and A2, (**b**) B1 and B2, (**c**) C, and (**d**) D and E observed in TMD simulations of VDR–VD3 system. The trajectories of ligand C8 atom (Fig. 1b) are shown

Computational details and structural analysis

The RAMD simulations were done using the AMBER 8.0 simulation package (Case et al. 2006) and the RAMD code implemented by Wade et al. (Ludemann et al. 2000). The 2.2 ns MD simulation of VD3 bound to the VDR LBD, and the TMD and SMD ligand unbinding simulations were done using the AMBER 9.0 simulation package (Case et al. 2006). In all the simulations, the ff99 force field (Cornell et al. 1995; Wang et al. 2000) augmented with the backbone corrections of Hornak et al. (2006) was used. The parameters of VD3 were generated with the Antechamber suite of AMBER 9.0 in conjunction with the general amber force field (Wang et al. 2004). The atomic point charges of the ligand were calculated with the two-stage RESP fit (Bayly et al. 1993; Duan et al. 2003) at the HF/6-31G* level using ligand geometry optimized at the same level using the Gaussian03 program (Frisch et al. 2003). The maximum protein RMSD values reported for ligand unbinding trajectories are the biggest RMSD moving averages of 30 structures, spanning 22.5 ps, calculated for protein backbone atoms (C, CA, N) using the starting structure of each trajectory as a reference. Ligand unbinding pathways were inspected visually by the VMD program (Humphrey et al. 1996). The protein structures of the figures were generated using the PyMOL program (DeLano Scientific 2008).

The following class 2 (Bain et al. 2007) NRs and their crystal structures were used in structural comparison: CAR (Protein Data Bank entry 1XVP), FXR (1OSV), LXRβ (1P8D), PPARγ (2PRG), PXR (1M13), RARγ (1FCY), RORβ (1K4 W), TRβ (1NQ0) and VDR (1IE9).

Results

Ligand unbinding pathways

To investigate the applicability of RAMD ligand unbinding simulations to economically identify the likely unbinding

pathways, a total of 360 RAMD simulations, starting from five structures (SS1–SS5) separated by 0.4 ns of the 2.2 ns MD simulation using four different RAMD parameter sets, were done for VDR–VD3 complex. In addition, to compare the VD3 unbinding pathways obtained from 10 to 200 ps RAMD simulations, 40 TMD unbinding simulations of 0.5–2.5 ns were done. In both the RAMD and TMD method ligand unbinding pathways are not predefined, so the pathways obtained are solely determined by the interactions of the simulation system.

Three main clusters (A-C, Fig. 2a–c) of VD3 unbinding pathways from the LBP of VDR were observed in the RAMD and TMD simulations. All the exit trajectories from TMD simulations are visualized in Fig. 2. The figure shows trajectories followed by C8 atom of the ligand (Fig. 1b). (RAMD trajectories of pathways A–C are depicted in Figs. S1–S3 of supplementary material). In the RAMD simulations clearly the most frequently observed pathways were A and B, found in 52 and 31% of the cases. The other pathways, C, D and E, were observed more rarely (3–8%). The same five pathways were observed also in the TMD simulations and in agreement with RAMD the pathways A and B were the most frequently observed, although in TMD the pathway C had clearly gained popularity. However, because of the small number of TMD simulations no firm conclusions about the relative preference of individual pathways can be made. In general, the exit pathways of the two methods were similar. The increased frequency of pathway C and subpathway A2 in the TMD simulations were the main differences between the RAMD and TMD simulations. This was most probably due to the slower, and more realistic, unbinding trajectories of the TMD simulations allowing longer time-scale structural changes to take place in the protein structure as the ligand explores possible exit channels.

Unbinding pathway A

In pathway A ligands exit from the LBP through a channel, which is created by rearrangement or dislocation of H12. This pathway, which can be divided in subpathways A1 and A2 (Fig. 2a), was the most frequently observed pathway in RAMD simulations. In the case of VDR and nuclear receptors in general, H12 is known to be flexible and in many cases probably disordered or dislocated from its agonistic position in the absence of ligand. Therefore, this channel represents a likely entry route for ligands to the LBP of NRs. It must be noted that in all the simulations of this work the H12 was initially in the agonistic conformation of the crystal structure (Tocchini-Valentini et al. 2001) in which it is tightly bound to the body of the protein. The RAMD simulations produced a rather wide funnel of exit pathways locating mainly between the C-terminal part of H12 and H11. In this pathway (A1) ligands exit so that H12 tends to stay in contact with the rest of the protein or only slightly displaced from the agonistic position. Typically, the ligand makes contacts with Tyr401 (H11), Phe422 (H12) and the hydrophobic H12 residues Leu414 and Val418 as it leaves the LBP. A small part of RAMD simulations and the majority of TMD simulations followed the subpathway A2 that required dislocation of H12 from its agonistic position and formation of an opening connecting the LBP to the surface of the protein. This opening is lined by His397 and Ser 398 (H10), Tyr401 (H11) and Phe422 (H12).

Unbinding pathway B

Pathway B is located in the opposite direction of the LPB compared to pathway A, close to the A ring of a bound VD3. This pathway has an opening at the protein surface between the H1–H2 loop and the short β-sheet between H5 and H6 (Fig 2b). It is characterized by a rather large funnel of exit paths, which can be divided in subpathways B1 and B2. In the RAMD simulations, subpathway B1 was slightly more frequently observed than B2. The outer surface opening of subpathway B1 is located in the C-terminal part of the H1–H2 loop lined by Tyr147, Phe150, Tyr293 and Cys288. The opening of B2 is located between the middle part of the H1–H2 loop and the β-sheet, lined by Tyr143, Tyr147 and Ser278. The ligand unbinding along pathway B typically involves structural changes in the flexible H1–H2 loop.

Unbinding pathways C–E

Unbinding pathway C runs through an opening formed by the H1–H2 loop and the middle part of H3 flanked by Tyr236 and Lys240 (Fig. 2c). On the basis of VDR–VD3 crystal structure this pathway seems a possible exit route as there exist several water molecules forming a hydrogen bonded water channel starting in the vicinity of the A ring of a bound natural ligand leading to the protein surface (Rochel et al. 2000; Tocchini-Valentini et al. 2001). Pathway C follows this water channel. Along this channel there are three aromatic residues, Tyr147 (H1–H2 loop), Phe150 (H2) and Tyr236 (H3), which form the walls of the exit channel. At the protein surface there are Asp144 (H1–H2 loop), Asp149 (H1–H2 loop) and Lys240 (H3) forming the rim of the channel opening. This pathway was observed only rarely in the RAMD simulations but more frequently in the TMD simulations.

Two additional pathways, D and E, were observed in the RAMD and TMD simulations (Fig. 2d). Pathway D is located between the β-sheet and H6 and H7, and pathway

E between H11 and the N-terminal part of H7. These exit routes lead to the dimerization surface of VDR and were observed rarely in the simulations. Therefore, they do not represent likely entry/exit pathways of VDR. In line with this, exit pathways reminiscent of D and E were observed in the RAMD unbinding study of all-*trans* retinoic acid from RARγ and were thought to represent unlikely unbinding pathways (Carlsson et al. 2006).

Different RAMD parameter sets

To study the effect of RAMD simulation parameters to the resulting unbinding pathways four sets of simulation parameters (Table 1) were tested. These sets were found in extensive test simulations to lead to ligand expulsions within 200 ps. Such rather short expulsion times could lead to unrealistically high forces, drastic changes in protein structures and, consequently, to non-natural ligand exit routes. However, compared to the reference TMD and SMD simulations, the exit routes obtained with RAMD seemed reasonable. The chosen RAMD protocol allowed carrying out a large number of simulations and thus to make conclusions about the feasibility of RAMD for objective exploration of possible unbinding pathways.

The number of trajectories following paths A–E with each parameter set is presented in Fig. 3 (Table S1, supplementary material). That the accuracy of the path distributions of Fig. 3 obtained from 40 simulations of each parameter set are useful in comparing the sets, is seen in the similarity of pathway distributions of set 4 in Fig. 3 and the distribution of all simulations of Fig. 4 ("All", Table S2, supplementary material). All simulations of Fig. 4 were calculated with the parameter set 4 (the 40 simulations of Fig. 3 are included in Fig. 4). The parameter set 4 was chosen for more extensive RAMD simulations listed in Table 3 because it provided exit pathway distribution close to the average of the tested parameters with reasonable number of new directions taken in unbinding trajectories. The parameter sets 2–4 of Fig. 3 show qualitatively similar distributions of unbinding pathways. The ratio of the most frequently observed paths A and B is 3:5 for sets 2 and 4, and 2.5:5 for the set 3. In contrast, the pathway A to B ratio is 1:1 for the set 1. This difference in pathway ratio is reflected in the lengths and especially in the number of new directions in RAMD simulations: the number of new directions in the set 1 simulations was on average 119.5, more than two times larger than the averages of sets 3 and 4, and 15 times larger than 8.2 of set 2 (Table 2). It is also notable that although ligand unbinding trajectories were rather straight in parameter set 2 simulations, as evidenced by small number new directions, the distribution of unbinding pathways is close to those of sets 2 and 3.

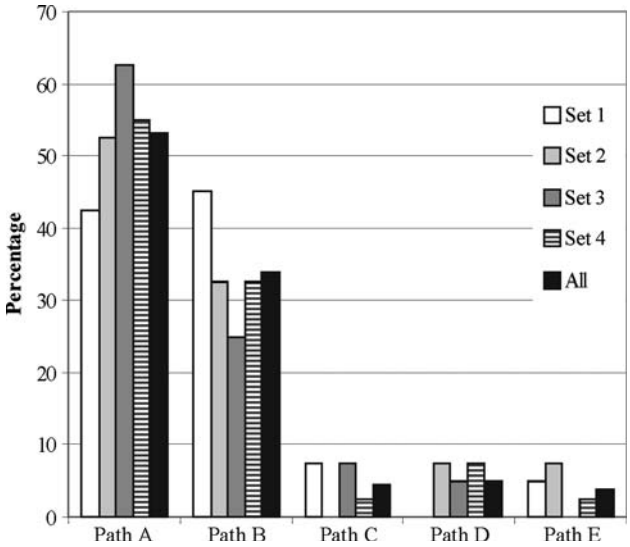

Fig. 3 Percentages of RAMD trajectories following paths A–E using parameter sets 1–4 ($n = 40$) and all trajectories ($n = 160$)

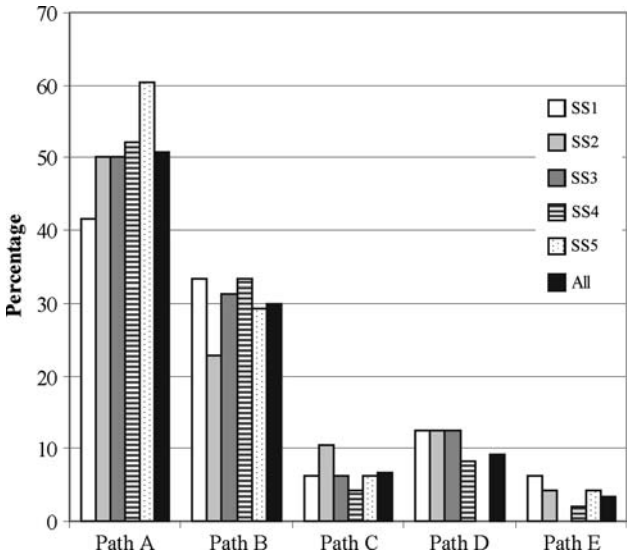

Fig. 4 Percentages of RAMD trajectories following paths A–E for starting structures SS1–SS5 ($n = 48$) and all trajectories ($n = 240$) using parameter set 4

Different RAMD starting structures

To study the effect of starting structures on unbinding pathway distributions, 40 RAMD simulations were done for each of the five starting structures (SS1–SS5) of the VDR–VD3 simulation using the parameter set 4. On the basis of Fig. 4 (supplementary material, Table S2), where the observed pathway distributions are presented for different starting structures, there seems to be a minor dependence between the pathway distributions and starting structures. This may be partly due to the rather compact structure of the VDR LBD and, consequently, small structural differences between the starting structures. In addition, the starting

Table 2 Average number of new directions, simulation lengths and maximum RMSDs in RAMD simulations using parameter sets 1−4

	Set 1 (n = 40)	Set 2 (n = 40)	Set 3 (n = 40)	Set 4 (n = 40)	All (n = 160)
Directions	119.5	8.2	54.3	43.3	56.3
Length (ps)	58.8	46.2	56.3	50.6	53.0
Max. RMSD (Å)	2.04	2.04	2.16	1.95	2.05

structures were separated at the most by 1.6 ns of simulation time, which is not expected to lead to large structural changes. The only notable difference in pathway distributions is the clearly smaller than average proportion of path A trajectories in SS1 (timepoint 0.6 ns) and larger than average proportion of path A trajectories in SS5 (timepoint 2.2 ns) simulations. Interestingly, use of these two starting structures resulted in shortest simulation times with smallest number of new directions (Table 3): the average length and number of new directions were 41.1 ps and 30.2 for SS1, and 43.9 ps and 34.0 for SS5 simulations, being clearly smaller than 53.8–78.0 ps and 62.2–79.7 of the other starting structures. The same observation was made in the simulations carried out in parameter set testing (supplementary material, Table S3 and S4). Otherwise no clear trends were observed in pathway distributions and RAMD simulation lengths. The differences in pathway distributions can not be explained by varying proportions of different pathways, because the average simulation lengths and the new directions in simulations following paths A–E listed in Table 4 show rather small differences, although the simulations leading to ligand unbinding along the most frequently observed paths A and B were somewhat shorter than the simulations following other pathways. A likely explanation for the difference in path distributions between SS1 and SS5 simulations is the increased likelihood of A and B pathways as the VDR–VD3 MD simulation progressed. This is seen in the increase in the sum of path A and B trajectories towards the later timepoint starting structures: the percentage share of these two pathways is 75.0, 81.3 and 89.6% for the starting structures SS1, SS3 and SS5, respectively.

Table 3 Average number of new directions, simulation lengths and maximum RMSDs in RAMD simulations for starting structures SS1–SS5 using parameter 4

	SS1 (n = 48)	SS2 (n = 48)	SS3 (n = 48)	SS4 (n = 48)	SS5 (n = 48)	All (n = 240)
Directions	30.2	78.0	53.8	60.2	34.0	51.3
Length (ps)	41.1	79.7	62.2	65.0	43.9	58.4
Max. RMSD (Å)	1.85	2.00	2.15	2.13	2.21	2.07

Table 4 Average number of new directions, simulation lengths and maximum RMSDs in RAMD simulations following paths A–E using parameter set 4

	A (n = 122)	B (n = 72)	C (n = 16)	D (n = 22)	E (n = 8)	All (n = 240)
Directions	49.8	52.3	50.9	55.5	54.0	51.3
Length (ps)	56.9	57.9	63.4	64.3	59.5	58.4
Max. RMSD (Å)	2.15	1.93	2.03	2.14	2.05	2.07

Unbinding pathways from TMD simulations

To study how reasonable the high-velocity ligand unbinding pathways obtained from the RAMD simulations are and to study the structural details of the unbinding pathways eight TMD simulations of 0.5–2.5 ns were started from each of the five starting structures. The summary of TMD simulations is presented in Table 5. The same five main unbinding pathways were found in the TMD and in the RAMD simulations. However, the TMD simulations indicated that there are two clear subpathways, presented in Fig. 2a, b, for paths A and B. The RAMD trajectories followed the both TMD subpathways of path B, although in RAMD simulations no separate clusters were visible. Subpathway A2 was not observed in the RAMD simulations, in which practically all ligands followed subpathway A1. A and B were the two most frequently observed pathways in the TMD and RAMD simulations, although, in contrast to RAMD, path B was more frequently observed than path A. However, it is more notable that in the TMD simulations the unbinding pathway C was observed in 20% of the trajectories, but in the RAMD simulation its share was only 7%. In addition, the path B to C ratio was 2:1 in TMD and 5:1 in RAMD simulations. This increase is notable, because the very first part of pathways B and C is shared. As can be seen from Fig. 2b and c, there is a bend in pathway C at the point where the two pathways diverge. Formation of unbinding channel C requires rotation of side chain torsion angles of Tyr147 (H1–H2 loop), Phe150 (H2) and Tyr236 (H3), which is presumably more likely to take place during the TMD than much shorter RAMD simulations. This is indirectly supported by the fact that average length of path C trajectories was 1.25 ns and that of path B 1.06 ns, indicating that slower unbinding rate promotes path C. The average maximum RMSDs are comparable for the three most frequently observed unbinding pathways A–C and higher for the more rarely observed D and E (Table 5). The RMSDs of TMD simulations were somewhat larger than those of the considerably shorter RAMD calculations (Table 2) simply showing that protein did not have time to respond to forced ligand expulsions of RAMD simulations.

Table 5 Summary of TMD simulations

Exit path	Number of trajectories ($n = 40$)	Average simulation length (ns)	Average maximum RMSD (Å)
A	11 (27.5)	1.36	2.21
B	16 (40.0)	1.06	2.36
C	8 (20.0)	1.25	2.27
D	2 (5)	1.25	2.66
E	3 (7.5)	1.83	2.48

Percentage values are in parentheses

In other words, in RAMD simulations ligand-induced structural changes stayed localized in the vicinity of the site where ligand caused protein distortion by the applied forces.

Force profiles from SMD simulations

The SMD simulations were done for the most plausible ligand unbinding pathways A, B and C found in the RAMD and TMD simulations to obtain quantitative estimates for the ligand unbinding force profiles. This would make it possible to compare the path distributions observed in the RAMD simulations with the preferences of the paths. It must be noted, however, that more extensive simulations with techniques providing free energy barriers should be carried out to obtain more reliable estimates about the relative preferences of ligand expulsion paths. Two subpathways were considered for path A (A1 and A2) and B (B1 and B2) (Fig. 2a, b). Based on the averages of the maximum forces (F_{max}) of the calculated force profiles, there are no large differences between the studied paths (Table 6; Fig. 5). However, path B2 has the lowest average F_{max} value, closely followed by B1. If the averages of the three lowest F_{max} values are considered, B2 has still the lowest maximum force, but other paths are now predicted to be equally favorable (Table 6). All the force profiles share similar 1,000–1,300 pN barrier in the beginning of the unbinding path at about 3.5–6 Å (Fig. 5). (Force profiles of individual trajectories are shown in supplementary material,

Table 6 Maximum forces (F_{max}) of the SMD ligand unbinding simulations along paths A1, A2, B1, B2 and C and the average F_{max} values

Exit path	F_{max} (pN)							Average[a]
A1	1,025	1,027	1,034	1,038	1,095	1,295	1,364	1,125 (1,029)
A2	1,017	1,034	1,051	1,061	1,126	1,200	1,214	1,100 (1,034)
B1	991	1,047	1,056	1,080	1,104	1,108	1,125	1,073 (1,031)
B2	941	957	1,005	1,094	1,119	1,134	1,176	1,061 (968)
C	1,028	1,039	1,062	1,063	1,085	1,169	1,195	1,092 (1,043)

Averages of the three lowest F_{max} trajectories are in parentheses

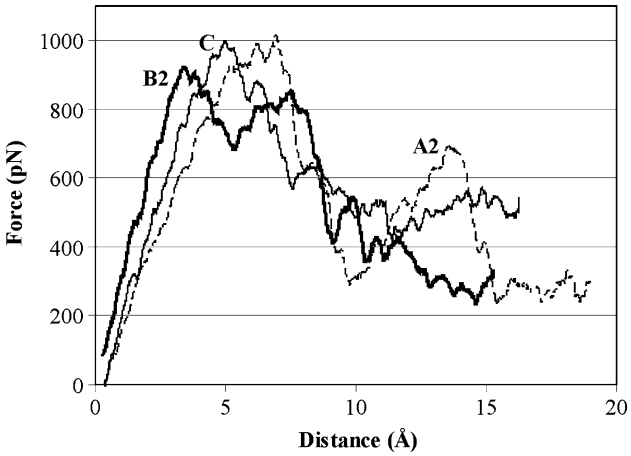

Fig. 5 Average force profiles for paths A2, B2 and C

Fig. 2. S4–S8.) At this point the six hydrogen bonds formed between the LBP and VD3 are broken. After the first barrier there exists a second barrier on path A and B, which is somewhat lower and less clearly defined for path B than A. In the case of path C, no such second barrier can be seen. In subpathway A1 and A2, there is a phase of notably low forces after the first barrier located at about 9–11 Å has been crossed. The second clearly lower barrier is located between 10 and 13 Å in the case of A1, and between 13 and 15 Å in the case of A2. At this point ligand is passing H12, which has to slightly rearrange and change conformation. The second barrier of path A1, which is the more favorable of the studied subpathways of path A, is ~700 pN. The second barrier of subpathways B1 and B2 has a clearly less defined position and height compared to that of path A. This is due to the rearrangement of the H1–H2 loop and its rather large mobility leads to varying barrier heights and positions. It is notable that two lowest F_{max} (~950 pN) unbinding trajectories were both found among the B2 simulations (Table 6). The force profiles of path C showed the most consistent behavior between the parallel simulations. After the first barrier the forces decreased as the ligand was pulled through the unbinding channel. The forces stayed rather high, yet below 700 pN. This was due to extensive interactions made by the ligand along the exit path.

On the basis of SMD simulations, path B2 seems to be the most favorable for VD3 unbinding from the LBP of VDR. The other pathways studied with the SMD method were similar in terms of F_{max} values.

Discussion

General

A prerequisite for investigation of ligand entry/exit pathways from protein LBP using quantitative computer simulation

methods (Aird et al. 2007; Lau and Roux 2007; Park et al. 2003; Xiong et al. 2006) is that the most likely pathways must be first somehow deduced. In favorable cases this can be accomplished just by visual inspection of the protein, but usually it is a more complicated task and calls for computational tools for objective pathway selection. The RAMD method (Ludemann et al. 1997), in which randomly oriented forces are imposed on the ligand to accelerate the finding of trajectories leading out of the LBP, seems a highly attractive approach to this purpose as evidenced by a number of successful applications (Ludemann et al. 1997, 2000; Schleinkofer et al. 2005; Wang and Duan 2007). To study the applicability of the RAMD method in finding the most likely unbinding pathways and the quality of the pathways found, a large number of RAMD simulations were done for VDR–VD3 system. In order to get statistically reliable number of unbinding trajectories, simulation parameters leading to rather short (<200 ps) exit trajectories were chosen. Short simulation times may be desirable when possible unbinding pathways are explored before starting more realistic simulations requiring slow ligand expulsion velocities and a number of parallel simulations for converged results. The structural features of the RAMD trajectories were compared to much long TMD simulations (0.5–2.5 ns), and pathway distributions of the RAMD simulations to force profiles calculated using the SMD method.

Comparison of RAMD with TMD and SMD

Simulations of this work suggested that quite a small number (50–100) of short RAMD unbinding simulations, preferably using slightly different simulation parameters, is enough to locate all five unbinding pathways (A–E) of VDR. However, short trajectories inevitably lead to pathways, which tend to be straighter than those found in the reference slow-velocity unbinding simulations using the TMD method. That all structural details of the RAMD trajectories are not shared by the low-velocity pathways, could be seen in the absence of subpathway A2 in the RAMD simulations but as a clear cluster of pathways in TMD simulations (Fig 2a). On the basis of SMD force profiles, A1 and A2 were estimated to be equally likely exit paths. Also the path C was underrepresented in the RAMD results. Thus, although RAMD can rather quickly reveal the most likely unbinding pathways, the exact pathways are not necessarily found with this methodology. This might not be a problem, because for example in SMD studies slightly different pulling directions and pathways must in any case be tested to be sure that the most favorable pathways have been identified.

It is tempting to speculate that if a sufficiently large number of RAMD simulations were carried out, the observed distribution of pathways would converge close to that deduced from quantitative energies obtained from, for example, SMD simulations. The comparison of the RAMD frequencies of paths A, B and C, which showed good enough convergence for this purpose (Figs. 3, 4), with the F_{max} values of the SMD simulations (Table 6) indicated that there is a qualitative agreement. The number of path C trajectories obtained from RAMD simulations was slightly larger than average when simulations were started from SS1 and SS2 structures, bringing the observed frequencies in better agreement with the conclusions based on SMD forces. This seems natural as the SMD simulations were started from the SS2 starting structure. In addition, because the RAMD simulations led to high unbinding velocities, the obtained distributions may show bias towards the probability the ligand has in entering a particular exit channel. This is likely to be the case for RAMD parameter set 2 simulations, in which on average only 8.2 new random directions were chosen during ligand expulsion, being considerably less than the average number 56.3 of all simulations (Table 2). This would mean that with parameter set 2, ligand will follow the first exit channel it enters. In spite of this, the pathway distribution with this set does not deviate much from the average distribution. Closest to set 2 in terms of pathway distribution is set 4, which has the second smallest number of new directions. In line with the above assumptions, these two sets have increased number of structurally unfeasible routes D and F. On the other hand, the distribution of parameter set 1, which has clearly the largest number of new directions (119.5), resembles most the distribution deduced from SMD results: the frequencies of paths A and B are practically equal. Thus, the comparison of the RAMD and SMD data indicates that in the unbinding path distributions of Figs. 3 and 4 there is a bias towards the probability of entering the exit channel. This conclusion is partly supported by the TMD simulation data (Table 5). In the TMD simulations, in which the ligand was expelled slowly (0.5–2.5 ns) out of the LBP, paths B and C were observed in the ratio of 2:1, in qualitative agreement with SMD results.

Ligand unbinding pathway A

According to the mouse trap model ligand binding leads to repositioning of H12 to the agonistic position, in which H12 is tightly packed against the core of the NR LBD and efficiently closes the LBP (Fig. 1a) (Li et al. 2003). NMR spectroscopy studies have shown that ligand binding stabilizes a large part of NR LBD, including H12 (Berger et al. 2003; Johnson et al. 2000). Even in the case of constitutively active NRs, which show considerable activity in the absence of ligand, H12 is more flexible in apo structures than in the receptor-agonist-complexes (Kallenberger et al. 2003). In the case of PPARγ increased fluctuations,

especially in the H12 region, are seen in the PPAR-partial agonist complexes compared to full agonist complexes (Bruning et al. 2007), and it has been observed that significant flexibility in the LBD may still remain even when an activating ligand is bound to the LBP (Chrencik et al. 2005). In addition, crystal structures of apo-LBD and antagonist-LBD structures of several NRs have shown that H12 may adopt several alternative conformations in which it does not block ligand entrance to the LBP and, thus, offers a low-energy entry channel for ligand binding (Kallenberger et al. 2003; Li et al. 2003; Nagy and Schwabe 2004). Thus, there is ample of experimental data indicating that a likely ligand exit/entry channel is located in H12 region when NR is in a non-active state. In line with this, even though H12 was placed in the agonistic conformation in the beginning of the ligand expulsion simulations of this work, exit through the H12 region (path A) was estimated to be a feasible alternative. Amino acid mutations, which decrease interactions between the H12 and the main body of VDR should facilitate ligand unbinding through path A. Good candidates for such residues are hydrophobic H12 residues Leu417, Val418, Val421 and Phe422 and H11 residue Tyr401. Alanine replacement of these residues has been found to considerably decrease VDR activation potency of VD3 (Väisänen et al. 2002; Yamamoto et al. 2006). It is interesting that in the earlier RAMD study on RARγ (Carlsson et al. 2006) no exit trajectories comparable to path A was found. Inspection of the RARγ crystal structures gives no simple explanation to this.

Ligand unbinding pathway C

Crystal structure analyses of NR LBDs have led to suggestions that there would be alternative ligand entry/exit pathways in addition to the H12 region. In the cases of TRα (Wagner et al. 1995) and PPARγ (Nolte et al. 1998), crystal structures revealed a putative ligand entry/exit site between H3 and the β-sheet (Fig. 6). In addition to the fact that the putative site is located in a less-dense part of LBD, the same region is the most flexible part of many NRs as suggested by large temperature factors and incomplete experimental electron densities (Martínez et al. 2006). An alternative site could offer a ligand exit route when the opening in the vicinity of H12 was blocked by bound co-regulator proteins (co-activator/co-repressor). The path between H3 and the β-sheet has been found earlier in RAMD ligand expulsion simulations of RARγ (Carlsson et al. 2006), LES simulations of TRα/β (Martínez et al. 2005) and TMD simulations of PPARγ (Genest et al. 2008). On the basis of SMD simulations, this route was found to be an energetically plausible entry/exit path for RARγ (Kosztin et al. 1999) and suggested to be the most likely pathway for ligand dissociation from the LBP of TRα/β

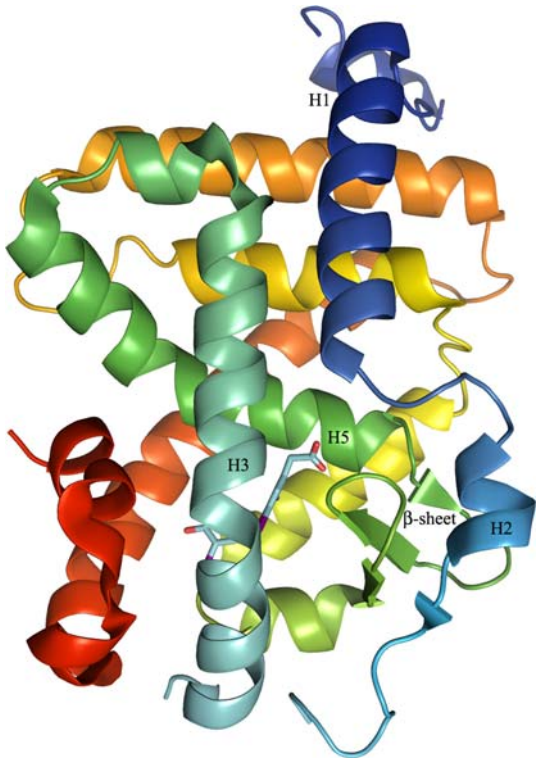

Fig. 6 Structure of TRβ (Protein Data Bank entry 1NQ0)

(Martínez et al. 2006). Interestingly, crystal structures of VDR-ligand complexes have revealed that in the same region of LBD, between H3 and the H1–H2 loop, there exists a possible ligand entry/exit channel. Namely, several water molecules are seen in the vicinity of the A ring of a bound VD3 forming a water channel connecting the LBP to the protein surface (Rochel et al. 2000; Tocchini-Valentini et al. 2001). This water channel, which follows path C, has been probed in VDR ligand design by making C-2α substituted VD3 analogs. Several such analogs showed high VDR affinity and crystal structure determinations revealed that even 3-hydroxy-1-propoxy substituent fits in the water channel and replaces bound water molecules (Hourai et al. 2006). Furthermore, in the case of VDR an alternative ligand biding pocket has been suggested to locate between H2 and the β-sheet (Mizwicki et al. 2004). This pocket, which has been suggested to be responsible for nongenomic rapid responses of VDR and to serve as an alternative ligand entry portal, is located close to the proposed entry/exit paths of TRα/β and PPARγ, and path C of this work. Thus, pathway C represents a structural feature shared by several NRs.

Ligand unbinding from VDR and TRα/β

The SMD force profiles suggested that ligand unbinding through the water channel of VDR (path C), which was the

only one of the studied pathways that did not have a secondary barrier on the force profile, was slightly less favorable than path B. In addition, in the RAMD and TMD simulations ligand unbinding was observed clearly more frequently to take place through path B than C. In contrast, in the case of TRα/β path C was calculated to be the most likely unbinding pathway. Comparison of the VDR (Tocchini-Valentini et al. 2001) (Fig. 2a) and TRβ (Huber et al. 2003) (Fig. 6) crystal structures provides a plausible explanation for this difference. In VDR, the path C is much narrower than in TR, and also in RAR, due to the close packing of H2 and the N-terminal part of H3, and the C-terminal part of H1 and the C-terminal part of H3. In the case of TR, the corresponding H3 packing is clearly less extensive creating a more flexible and less dense region between H3 and H1, H2 and the β-sheet. In TR, there is also a conserved Pro residue in the middle of H3, which increases the tendency of the helix to break into small α helices and promote ligand escape through this route (Martínez et al. 2005). This is seen as a small bend and structural irregularity in the vicinity of the conserved Pro of H3 (Huber et al. 2003) (Fig. 6). In addition, in TR the B route is blocked by the β-sheet, which enters between H2 and H5. In VDR an opening may be formed between the flexible H1–H2 loop and the β-sheet. As a consequence of these structural differences, path C becomes less favorable and path B more favorable for VDR compared to TR, and provides a structural explanation for the observed difference in the likelihood of the unbinding paths B and C in the two NRs.

Amino acids residues, whose mutations would selectively affect ligand unbinding through alternative paths can be suggested based on the simulations of this work. Such mutations would change unbinding kinetics and help experimentally verifying which unbinding paths are actually used. The H12 destabilizing residues, discussed above, are obvious candidates in probing path A unbinding. Ligand unbinding through path B requires that an opening is formed between Tyr147, Cys288, Tyr293 and Tyr295 and, thus, mutations of these residues would facilitate unbinding following path B. In the case of path C, interactions between Phe150, Phe153, Leu233 and Tyr236, which form an interconnected hydrophobic patch of residues, are disrupted. Most of these mutations are known to be important for the activity of VDR (Väisänen et al. 1998, Yamamoto et al. 2006).

The relative likelihood of alternative exit pathways from NR LBP is affected by the chemical nature of the ligand. For example, in the case of TRα/β simulations suggested that different ligands favor different unbinding pathways (Martínez et al. 2005). This behavior is likely to depend on ligands' interactions with protein and solvent along exit pathways (Martínez et al. 2006). The path C of VDR follows the water channel observed in the crystal structures. Thus, a ligand having hydrophilic substituent in this region would probably prefer path C more than VD3. One such candidate is lithocholic acid, an endogenous VDR ligand, having a highly hydrophilic carboxylate functional group (Makishima et al. 2002). Ligand docking studies have suggested that lithocholic acid binds to VRD LBP so that its carboxylate group is positioned close to the entry of the water channel (Jurutka et al. 2005). This would increase lithocholic acid's preference to path C unbinding.

Implications to class 2 nuclear receptors

VDR and TRs belong to class 2 NRs (Bain et al. 2007; Olefsky 2001), which typically exist as heterodimers with RXR. These receptors bind as dimers to the response elements of the target genes and tend to stay bound to DNA with and without a ligand. Thus, as a dimer the RXR of the heterodimer blocks ligand entry/exit through paths D and E, as the helices 7, 9, 10 and 11 contribute to the dimerization surface. That dimerization changes the preference of ligand unbinding paths has been shown in recent LES simulations of ERα monomer and dimer (Sonoda et al. 2008). On the other hand, co-activator proteins recognize the activation function 2 region of the LBD by a recognition helix, which binds in a groove formed between helices 3, 4 and 12. Therefore, co-activator binding most likely fixes H12 to the agonistic position and closes path A. This suggests that a second ligand binding/unbinding channel, in addition to H12 region, might have functional role in the case of class 2 NRs. If this is the case, one would expect that class 2 NRs had common structural features in their LBDs favoring ligand binding/unbinding through path B (VDR) or path C (TRα/β). Based on the phylogenetic analysis the class 2 NRs can be divided in two subfamilies, 1 and 4 (Escriva et al. 2000; Laudet 1997; Zhang et al. 2004). The vast majority of class 2 NRs belong to subfamily 1, which can be further divided into groups. VDR belongs with PXR and CAR to group 1I and TRα/β to group 1A. Crystal structures of LBDs of NRs known to form heterodimers with RXR are available for representatives of six groups. Interestingly, all representatives of groups 1H (LXRs and FXRs) and 1I (VDR, PXR and CAR) have the H1, H2, H3 and β-sheet region arranged like in VDR, and all representatives of groups 1A (TRs), 1B (RARs), 1C (PPARs), and 1F (RORs) have the same region like in TRα/β. Thus, class 2 NRs forming heterodimers with RXR have their LBDs structurally conserved so that the putative ligand binding/unbinding pathways B and C exist in analogy to VDR or TRα/β. However, whether such an alternative entry/exit pathway, in addition to the channel regulated by the H12 mobility, is actually used in natural environment and has functional importance is not known and waits for experimental verification.

Conclusions

In this work, the applicability of RAMD for rapid exploration of VD3 unbinding pathways from the ligand-binding pocket of VDR was investigated. The TMD and SMD methods were used in generating reference low-velocity exit trajectories (TMD) and estimates for relative preferences (SMD) of the most relevant pathways. It was found that even though rather short RAMD simulations (<200 ps) were done, the main exit pathways with qualitatively correct relative preferences were produced. On the basis of VDR–VD3 system this requires that adequately large number of RAMD simulations (50–100) are done using RAMD parameters which result in not too straight ligand unbinding trajectories. Namely, it was observed that RAMD parameters, which led to trajectories with largest number of new directions, produced path distributions closest to that deduced from SMD force profiles. It is also beneficial if different starting structures are used.

Based on the results of this work, and earlier ligand unbinding studies on NRs using different simulation techniques, three common entry/exit paths have been identified. The most obvious one is located in the H12 region and is regulated by the H12 mobility. The other two paths are located in the structurally variable and flexible part of NRs close to the H1–H2 loop, the β-sheet and H3. The results obtained from the RAMD, TMD and SMD ligand unbinding simulations suggested that for VDR the unbinding pathway between the H1–H2 loop and the β-sheet between H5 and H6 is more favorable than the pathway locating between the H1–H2 loop and H3. The latter pathway has been earlier suggested, based on SMD simulations, to be the most likely exit path for TRα/β. Comparison of VDR and TRβ crystal structures revealed that this difference is due to slightly different packing of H1, H2, H3 and the β-sheet leading to formation of exit channels on different sides of H1–H2 loop. Crystal structures of other class 2 NRs showed that these NRs can be structurally divided in two groups: those having the H1, H2, H3 and the β-sheet region arranged like in VDR (Path B) or like in TRα/β (path C). Thus, the putative ligand entry/exit paths B and C identified by computer simulation techniques and by analyzing NR crystal structures seem to be a common feature shared by class 2 NRs.

References

Aird A, Wrachtrup J, Schulten K, Tietz C (2007) Possible pathway for ubiquinone shuttling in rhodospirillum rubrum revealed by molecular dynamics simulation. Biophys J 92:23–33. doi:10.1529/biophysj.106.084715

Bain DL, Heneghan AF, Connaghan-Jones KD, Miura MT (2007) Nuclear receptor structure: implications for function. Annu Rev Physiol 69:201–220. doi:10.1146/annurev.physiol.69.031905.160308

Bayly CI, Cieplak P, Cornell WD, Kollman PA (1993) A well-behaved electrostatic potential based method using charge restraints for deriving atomic charges—the resp model. J Phys Chem 97:10269–10280. doi:10.1021/j100142a004

Berger JP, Petro AE, Macnaul KL, Kelly LJ, Zhang BB, Richards K et al (2003) Distinct properties and advantages of a novel peroxisome proliferator-activated protein gamma selective modulator. Mol Endocrinol 17:662–676. doi:10.1210/me.2002-0217

Blondel A, Renaud JP, Fischer S, Moras D, Karplus M (1999) Retinoic acid receptor: a simulation analysis of retinoic acid binding and the resulting conformational changes. J Mol Biol 291:101–115. doi:10.1006/jmbi.1999.2879

Bruning JB, Chalmers MJ, Prasad S, Busby SA, Karnenecka TM, He YJ et al (2007) Partial agonists activate PPAR gamma using a helix 12 independent mechanism. Structure 15:1258–1271. doi:10.1016/j.str.2007.07.014

Carlsson P, Burendahl S, Nilsson L (2006) Unbinding of retinoic acid from the retinoic acid receptor by random expulsion molecular dynamics. Biophys J 91:3151–3161. doi:10.1529/biophysj.106.082917

Case DA, Darden TA, Cheatham TA III, Simmerling CL, Wang J, Duke RE, Ross WS, Kollman PA (2006) AMBER 9, University of California, San Francisco

Chawla A, Repa JJ, Evans RM, Mangelsdorf DJ (2001) Nuclear receptors and lipid physiology: opening the X-files. Science 294:1866–1870. doi:10.1126/science.294.5548.1866

Chrencik JE, Orans J, Moore LB, Xue Y, Peng L, Collins JL et al (2005) Structural disorder in the complex of human pregnane X receptor and the macrolide antibiotic rifampicin. Mol Endocrinol 19:1125–1134. doi:10.1210/me.2004-0346

Cornell WD, Cieplak P, Bayly CI, Gould IR, Merz KM, Ferguson DM et al (1995) A 2nd generation force-field for the simulation of proteins, nucleic-acids, and organic-molecules. J Am Chem Soc 117:5179–5197. doi:10.1021/ja00124a002

DeLano Scientific (2008) The PyMOL molecular graphics system, Palo Alto, CA

Duan Y, Wu C, Chowdhury S, Lee MC, Xiong GM, Zhang W et al (2003) A point-charge force field for molecular mechanics simulations of proteins based on condensed-phase quantum mechanical calculations. J Comput Chem 24:1999–2012. doi:10.1002/jcc.10349

Einstein M, Akiyama TE, Castriota GA, Wang CF, McKeewer B, Mosley RT et al (2008) The differential interactions of peroxisome profilerator-activated receptor γ ligands with tyr473 is a physical basis for their unique biological activities. Mol Pharmacol 73:62–74. doi:10.1124/mol.107.041202

Escriva H, Delaunay F, Laudet V (2000) Ligand binding and nuclear receptor evolution. Bioessays 22:717–727 doi :10.1002/1521-1878(200008)22:8<717::AID-BIES5>3.0.CO;2-I

Frisch MJ, Trucks GW, Schlegel HB, Scuseria GE, Robb MA, Cheeseman JR et al (2003) Gaussian 03, Revision B.04. Gaussian, Inc, Wellingford

Genest D, Garnier N, Arrault A, Marot C, Morin-Allory L, Genest M (2008) Ligand-escape pathways from the ligand-binding domain of PPAR gamma receptor as probed by molecular dynamics simulations. Eur Biophys J 37:369–379. doi:10.1007/s00249-007-0220-9

Gullingsrud JR, Braun R, Schulten K (1999) Reconstructing potentials of mean force through time series analysis of steered molecular dynamics simulations. J Comput Phys 151:190–211. doi:10.1006/jcph.1999.6218

Hornak V, Abel R, Okur A, Strockbine B, Roitberg A, Simmerling C (2006) Comparison of multiple amber force fields and development of improved protein backbone parameters. Proteins 65:712–725. doi:10.1002/prot.21123

Hourai S, Fujishima T, Kittaka A, Suhara Y, Takayama H, Rochel N et al (2006) Probing a water channel near the A-ring of

receptor-bound 1 alpha, 25-dihydroxyvitamin D3 with selected 2 alpha-substituted analogues. J Med Chem 49:5199–5205. doi:10.1021/jm0604070

Huber BR, Desclozeaux M, West BL, Cunha-Lima ST, Nguyen HT, Baxter JD et al (2003) Thyroid hormone receptor-beta mutations conferring hormone resistance and reduced corepressor release exhibit decreased stability in the N-terminal ligand-binding domain. Mol Endocrinol 17:107–116. doi:10.1210/me.2002-0097

Humphrey W, Dalke A, Schulten K (1996) VMD—visual molecular dynamics. J Mol Graph 14:33–38. doi:10.1016/0263-7855(96)00018-5

Hurth KM, Nilges MJ, Carlson KE, Tamrazi A, Belford RL, Katzenellenbogen JA (2004) Ligand-induced changes in estrogen receptor conformation as measured by site-directed spin labeling. Biochemistry 43:1891–1907. doi:10.1021/bi035566p

Isralewitz B, Gao M, Schulten K (2001) Steered molecular dynamics and mechanical functions of proteins. Curr Opin Struct Biol 11:224–230. doi:10.1016/S0959-440X(00)00194-9

Izrailev S, Stepaniants S, Isralewitz B, Kosztin D, Lu H, Molnar F et al (1998) Steered molecular dynamics. In: Deuflhard P, Hermans K, Leimkuhler B, Mark AE, Reich S, Skeel RD (eds) Computational molecular dynamics: challenges, methods, ideas, vol 4. Springer, Berlin, pp 39–65

Jarzynski C (1997) Nonequilibrium equality for free energy differences. Phys Rev Lett 78:2690–2693. doi:10.1103/PhysRevLett.78.2690

Jurutka PW, Thompson PD, Whitfield GK, Eichhorst KR, Hall N, Dominguez CE et al (2005) Molecular and functional comparison of 1, 25-dihydroxyvitamin D-3 and the novel vitamin D receptor ligand, lithocholic acid, in activating transcription of cytochrome P450 3A4. J Cell Biochem 94:917–943. doi:10.1002/jcb.20359

Johnson BA, Wilson EM, Li Y, Moller DE, Smith RG, Zhou GC (2000) Ligand-induced stabilization of PPAR gamma monitored by NMR spectroscopy: Implications for nuclear receptor activation. J Mol Biol 298:187–194. doi:10.1006/jmbi.2000.3636

Kallenberger BC, Love JD, Chatterjee VKK, Schwabe JWR (2003) A dynamic mechanism of nuclear receptor activation and its perturbation in a human disease. Nat Struct Biol 10:136–140. doi:10.1038/nsb892

Kosztin D, Izrailev S, Schulten K (1999) Unbinding of retinoic acid from its receptor studied by steered molecular dynamics. Biophys J 76:188–197

Lau AY, Roux B (2007) The free energy landscapes governing conformational changes in a glutamate receptor ligand-binding domain. Structure 15:1203–1214. doi:10.1016/j.str.2007.07.015

Laudet V (1997) Evolution of the nuclear receptor superfamily: early diversification from an ancestral orphan receptor. J Mol Endocrinol 19:207–226. doi:10.1677/jme.0.0190207

Li Y, Lambert MH, Xu HE (2003) Activation of nuclear receptors: a perspective from structural genomics. Structure 11:741–746. doi:10.1016/S0969-2126(03)00133-3

Ludemann SK, Carugo O, Wade RC (1997) Substrate access to Cytochrome P450cam: a comparison of a thermal motion pathway analysis with molecular dynamics simulation data. J Mol Model 3:369–374. doi:10.1007/s008940050053

Ludemann SK, Lounnas V, Wade RC (2000) How do substrates enter and products exit the buried active site of cytochrome P450cam? 1. Random expulsion molecular dynamics investigation of ligand access channels and mechanisms. J Mol Biol 303:797–811. doi:10.1006/jmbi.2000.4154

Makishima M, Lu TT, Xie W, Whitfield GK, Domoto H, Evans RM et al (2002) Vitamin D receptor as an intestinal bile acid sensor. Science 296:1313–1316. doi:10.1126/science.1070477

Margeat E, Bourdoncle A, Margueron R, Poujol N, Cavailles V, Royer C (2003) Ligands differentially modulate the protein interactions of the human estrogen receptors alpha and beta. J Mol Biol 326:77–92. doi:10.1016/S0022-2836(02)01355-4

Martínez L, Sonoda MT, Webb P, Baxter JD, Skaf MS, Polikarpov I (2005) Molecular dynamics simulations reveal multiple pathways of ligand dissociation from thyroid hormone receptors. Biophys J 89:2011–2023. doi:10.1529/biophysj.105.063818

Martínez L, Webb P, Polikarpov I, Skaf MS (2006) Molecular dynamics simulations of ligand dissociation from thyroid hormone receptors: evidence of the likeliest escape pathway and its implications for the design of novel ligands. J Med Chem 49:23–26. doi:10.1021/jm050805n

Mizwicki MT, Keidel D, Bula CM, Bishop JE, Zanello LP, Wurtz JM et al (2004) Identification of an alternative ligand-binding pocket in the nuclear vitamin D receptor and its functional importance in 1 alpha, 25(OH)(2)-vitamin D-3 signaling. Proc Natl Acad Sci USA 101:12876–12881. doi:10.1073/pnas.0403606101

Moras D, Gronemeyer H (1998) The nuclear receptor ligand-binding domain: structure and function. Curr Opin Cell Biol 10:384–391. doi:10.1016/S0955-0674(98)80015-X

Nagy L, Schwabe JWR (2004) Mechanism of the nuclear receptor molecular switch. Trends Biochem Sci 29:317–324. doi:10.1016/j.tibs.2004.04.006

Nettles KW, Sun J, Radek JT, Sheng SB, Rodriguez AL, Katzenellenbogen JA et al (2004) Allosteric control of ligand selectivity between estrogen receptors alpha and beta: implications for other nuclear receptors. Mol Cell 13:317–327. doi:10.1016/S1097-2765(04)00054-1

Nolte RT, Wisely GB, Westin S, Cobb JE, Lambert MH, Kurokawa R et al (1998) Ligand binding and co-activator assembly of the peroxisome proliferator-activated receptor-gamma. Nature 395:137–143. doi:10.1038/25931

Olefsky JM (2001) Nuclear receptor minireview series. J Biol Chem 276:36863–36864. doi:10.1074/jbc.R100047200

Park S, Khalili-Araghi F, Tajkhorshid E, Schulten K (2003) Free energy calculation from steered molecular dynamics simulations using Jarzynski's equality. J Chem Phys 119:3559–3566. doi:10.1063/1.1590311

Rochel N, Wurtz JM, Mitschler A, Klaholz B, Moras D (2000) The crystal structure of the nuclear receptor for vitamin D bound to its natural ligand. Mol Cell 5:173–179. doi:10.1016/S1097-2765(00)80413-X

Ryckaert JP, Ciccotti G, Berendsen HJC (1977) Numerical integration of cartesian equations of motion of a system with constraints: molecular dynamics of n-alkanes. J Comput Phys 23:327–341. doi:10.1016/0021-9991(77)90098-5

Schleinkofer K, Sudarko, Winn PJ, Ludemann SK, Wade RC (2005) Do mammalian cytochrome P450 s show multiple ligand access pathways and ligand channelling? EMBO Rep 6:584–589. doi:10.1038/sj.embor.7400420

Schlitter J, Engels M, Kruger P (1994) Targeted molecular-dynamics—a new approach for searching pathways of conformational transitions. J Mol Graph 12:84–89. doi:10.1016/0263-7855(94)80072-3

Schlitter J, Engels M, Kruger P, Jacoby E, Wollmer A (1993) Targeted molecular-dynamics simulation of conformational change—application to the T↔R transition in insulin. Mol Simul 10:291–308. doi:10.1080/08927029308022170

Shiau AK, Barstad D, Radek JT, Meyers MJ, Nettles KW, Katzenellenbogen BS et al (2002) Structural characterization of a subtype-selective ligand reveals a novel mode of estrogen receptor antagonism. Nat Struct Biol 9:359–364

Sonoda MT, Martínez L, Webb P, Skaf MS, Polikarpov I (2008) Ligand dissociation from estrogen receptor is mediated by receptor dimerization: evidence from molecular dynamics simulations. Mol Endocrinol 22:1565–1578. doi:10.1210/me.2007-0501

Tocchini-Valentini G, Rochel N, Wurtz JM, Mitschler A, Moras D (2001) Crystal structures of the vitamin D receptor complexed to superagonist 20-epi ligands. Proc Natl Acad Sci USA 98:5491–5496. doi:10.1073/pnas.091018698

Väisänen S, Rouvinen J, Mäenpää PH (1998) Putative helices 3 and 5 of the human vitamin D_3 receptor are important for the binding of calcitriol. FEBS Lett 440:203–307. doi:10.1016/S0014-5793(98)01436-7

Väisänen S, Peräkylä M, Kärkkäinen JI, Steinmeyer A, Carlberg C (2002) Critical role of helix 12 of the vitamin D_3 receptor for the partial agonism of carboxylic ester antagonists. J Mol Biol 315:229–238. doi:10.1006/jmbi.2001.5225

Wagner RL, Apriletti JW, McGrath ME, West BL, Baxter JD, Fletterick RJ (1995) A structural role for hormone in the thyroid hormone receptor. Nature 378:690–697. doi:10.1038/378690a0

Wang JM, Cieplak P, Kollman PA (2000) How well does a restrained electrostatic potential (RESP) model perform in calculating conformational energies of organic and biological molecules? J Comput Chem 21:1049–1074 10.1002/1096-987X(200009)21:12<1049::AID-JCC3>3.0.CO;2-F

Wang JM, Wolf RM, Caldwell JW, Kollman PA, Case DA (2004) Development and testing of a general amber force field. J Comput Chem 25:1157–1174. doi:10.1002/jcc.20035

Wang T, Duan Y (2007) Chromophore channeling in the G-protein coupled receptor rhodopsin. J Am Chem Soc 129:6970–6971. doi:10.1021/ja0691977

Xiong H, Crespo A, Marti M, Estrin D, Roitberg AE (2006) Free energy calculations with non-equilibrium methods: applications of the Jarzynski relationship. Theor Chem Acc 116:338–346. doi:10.1007/s00214-005-0072-2

Yamamoto K, Abe D, Yoshimoto N, Choi M, Yamagishi K, Tokiwa H et al (2006) Vitamin D receptor: ligand recognition and allosteric network. J Med Chem 49:1313–1324. doi:10.1021/jm050795q

Zhang ZD, Burch PE, Cooney AJ, Lanz RB, Pereira FA, Wu JQ et al (2004) Genomic analysis of the nuclear receptor family: new insights into structure, regulation, and evolution from the rat genome. Genome Res 14:580–590. doi:10.1101/gr.2160004